

Diagnosis of electron temperature of copper foil plasmas produced at the Shenguang-II facility

Chenglong Zhang(张成龙), Haochen Gu(谷昊琛), Yu Dai(戴羽), Ke Fang(方可), Yufeng Dong(董玉峰), Peng Zhou(周鹏), Yingjun Li(李英骏)

Citation: Chin. Phys. B, 2025, 34 (**7**): 075202. DOI: 10.1088/1674-1056/adca19
http://cpb.iphy.ac.cn; http://iopscience.iop.org/cpb

What follows is a list of articles you may be interested in

Comparative study of boron and neon injections on divertor heat fluxes using SOLPS-ITER simulations

Lei Peng(彭磊), Zhen Sun(孙震), Ji-Zhong Sun(孙继忠), Rajesh Maingi, Fang Gao(高放), Xavier Bonnin, Hua-Yi Chang(常华溢), Wei-Kang Wang(汪炜康), and Jin-Yuan Liu(刘金远)
Chin. Phys. B, 2024, 33 (**11**): 115201. DOI: 10.1088/1674-1056/ad711e

Experimental studies of H_2/Ar plasma in a cylindrical inductive discharge with an expansion region

Shi-Bo Li(李世博), Si-Yu Xing(邢思雨), Fei Gao(高飞), and You-Nian Wang(王友年)
Chin. Phys. B, 2024, 33 (**10**): 105201. DOI: 10.1088/1674-1056/ad6250

Long radial coherence of electron temperature fluctuations in non-local transport in HL-2A plasmas

Zhongbing Shi(石中兵), Kairui Fang(方凯锐), Jingchun Li(李景春), Xiaolan Zou(邹晓岚), Zhaoyang Lu(卢兆旸), Jie Wen(闻杰), Zhanhui Wang(王占辉), Xuantong Ding(丁玄同), Wei Chen(陈伟), Zengchen Yang(杨曾辰), Min Jiang(蒋敏), Xiaoquan Ji(季小全), Ruihai Tong(佟瑞海), Yonggao Li(李永高), Peiwan Shi(施陪万), Wulyv Zhong(钟武律), and Min Xu(许敏)
Chin. Phys. B, 2024, 33 (**2**): 025202. DOI: 10.1088/1674-1056/ad1093

Transition from a filamentary mode to a diffuse one with varying distance from needle to stream of an argon plasma jet

Hui-Min Xu(许慧敏), Jing-Ge Gao(高敬格), Peng-Ying Jia(贾鹏英), Jun-Xia Ran(冉俊霞), Jun-Yu Chen(陈俊宇), and Jin-Mao Li(李金懋)
Chin. Phys. B, 2024, 33 (**1**): 015205. DOI: 10.1088/1674-1056/ad0149

Theoretical analyses on the one-dimensional charged particle transport in a decaying plasma under an electrostatic field

Yao-Ting Wang(汪耀庭), Xin-Li Sun(孙鑫礼), Lan-Yue Luo(罗岚月), Zi-Ming Zhang(张子明), He-Ping Li(李和平), Dong-Jun Jiang(姜东君), and Ming-Sheng Zhou(周明胜)
Chin. Phys. B, 2023, 32 (**9**): 095201. DOI: 10.1088/1674-1056/ace033

Diagnosis of electron temperature of copper foil plasmas produced at the Shenguang-II facility

Chenglong Zhang(张成龙)[1,2], Haochen Gu(谷昊琛)[2,3], Yu Dai(戴羽)[2,3], Ke Fang(方可)[2], Yufeng Dong(董玉峰)[2,3], Peng Zhou(周鹏)[4,5], and Yingjun Li(李英骏)[1,†]

[1] *State Key Laboratory for Tunnel Engineering, China University of Mining and Technology, Beijing* 100083, *China*
[2] *Beijing National Laboratory for Condensed Matter Physics, Institute of Physics, Chinese Academy of Sciences, Beijing* 100190, *China*
[3] *School of Physical Sciences, University of Chinese Academy of Sciences, Beijing* 100049, *China*
[4] *Key Laboratory for Laser Plasmas (MoE) and School of Physics and Astronomy, Shanghai Jiao Tong University, Shanghai* 200240, *China*
[5] *Collaborative Innovation Center of IFSA (CICIFSA), Shanghai Jiao Tong University, Shanghai* 200240, *China*

(Received 10 February 2025; revised manuscript received 28 March 2025; accepted manuscript online 8 April 2025)

Warm dense plasmas are crucial for high-energy-density physics and inertial confinement fusion research. Experiments involving laser-irradiated copper (Cu) foil were performed at the Shenguang-II facility. A highly oriented pyrolytic graphite crystal spectrometer measured the time-integrated spectral distribution of Cu under varying laser intensities. Using the two-dimensional radiation-hydrodynamics code FLASH and the spectral analysis code FLYCHK, we simulated the temporal evolution of plasma density and temperature distributions, as well as the emission intensities of spectral lines at different temperatures and densities. The simulation results revealed that the two-electron satellite lines (J) and the resonance line (W) emissions of Cu originate predominantly from the radiation region near the critical density surface, with a density range from approximately 0.5 n_c to 1.0 n_c, and radiate primarily during the laser irradiation period. By analyzing the J/W intensity ratio of the measured spectral lines, we estimated the electron temperatures near the critical-density surface under different laser intensities.

Keywords: electron temperature, crystal spectrometer, x-ray spectroscopy

PACS: 52.57.–z, 52.57.Kk

DOI: 10.1088/1674-1056/adca19 **CSTR:** 32038.14.CPB.adca19

1. Introduction

Accurate diagnostics of warm dense plasma[1] are essential for diverse environments, ranging from magnetic confinement fusion and laser-produced laboratory plasmas[2,3] to astrophysical objects[4,5] such as supernova remnants and solar flares. Among the fundamental parameters characterizing plasma states, electron temperature and density are particularly critical for understanding plasma behavior and properties.

In experiments with high neutron yield, the temperature and density of fuel can be inferred from neutron yield diagnostics and neutron energy spectrum analysis.[6,7] For experiments without measurable neutron yields, alternative diagnostic approaches are employed. Plasma density is typically obtained through x-ray radiography,[8–11] while temperature measurements are conducted using x-ray spectroscopy.[12] As a non-invasive diagnostic tool, x-ray spectroscopy has become a widespread application in inertial confinement fusion (ICF) research. This technique enables plasma characterization by detecting characteristic emission spectral lines of specific elements. These spectral lines demonstrate high sensitivity to plasma conditions, primarily due to their dependence on atomic level populations, which are directly influenced by the plasma physical parameters. The intensity and spectral line shapes of these characteristic emissions are particularly responsive to variations in plasma conditions, making x-ray spectroscopy a powerful diagnostic tool in plasma physics research.

In experiments conducted by Beier *et al.*, high-contrast relativistic lasers irradiated μm thick Cu foils. High-resolution spectral analysis of x-ray emission reveals uniform heating up to 3.0 keV over 1 μm depths.[13] At the National Ignition Facility (NIF), high-resolution x-ray spectroscopy was employed to study the evolution of hot-spot plasma in indirect-drive ignition experiments. Gao *et al.* measured time-resolved Kr Heβ spectra. They derived electron densities and temperatures from Stark broadening and satellite line intensities, thus investigating the effect of W dopants in the ablator on hot-spot parameters.[14] X-ray spectroscopy has also been utilized to measure electron temperatures in direct-drive ignition schemes. Recently, Dai *et al.* performed double-cone ignition experiments[15] using Cl-doped targets. After heating the colliding plasma with fast electrons, they observed x-ray spectra of Cl. Employing radiation-hydrodynamics simulations and spectral calculations to replicate and diagnose the colliding plasma, the heated plasma temperature is estimated to be 600 eV ± 50 eV through comparison of experimental and simulated results.[16]

†Corresponding author. E-mail: lyj@aphy.iphy.ac.cn

© 2025 Chinese Physical Society and IOP Publishing Ltd. All rights, including for text and data mining, AI training, and similar technologies, are reserved.

In this paper, we demonstrate experimental measurements of Cu characteristic spectral lines obtained under varying laser conditions at the Shenguang-II facility. Through a combined analysis of experimental spectral line intensities and numerical simulations, we estimate the plasma temperature near the critical density surface under different experimental configurations.

2. Experimental setup and experimental results

The experiments were conducted at the Shenguang-II facility, as illustrated in Fig. 1. A 25 μm thick Cu foil (2 mm × 2 mm) was oriented perpendicular to the due south direction. Characteristic x-rays emitted from the target were collected using a highly oriented pyrolytic graphite (HOPG) flat crystal spectrometer,[17] positioned at 22.5° southwest of the equatorial plane. Two laser beams, located 22.5° above and below the spectrometer, were focused onto the Cu foil with a wavelength of 0.351 μm, corresponding to a plasma critical density of $n_c = 9.74 \times 10^{21}$ cm^{-3}. The x-ray spot size was characterized using a pinhole camera equipped with a 15 μm Al filter and image plate (IP) detectors, which provided a magnification of 6.56. A pinhole streak camera[18] was positioned due east to monitor x-ray emission dynamics during laser irradiation. A composite filter, consisting of a 2 μm Al layer and a 200 nm mylar film, was installed before the detector to attenuate visible light and low-energy photons, thereby improving the signal-to-noise ratio. A sequence of temporal pulses was generated by a reference laser and transmitted to the slit through an ultraviolet (UV) fiber, as shown in Fig. 4(c), serving as an additional time reference during experimental measurements. Table 1 summarizes the laser parameters used in the experiments. The HOPG crystal spectrometer covered an energy range of 7950 eV–8450 eV with a spectral resolution of ∼ 20 eV. Time-integrated x-ray spectroscopy was obtained using IP detectors.[19]

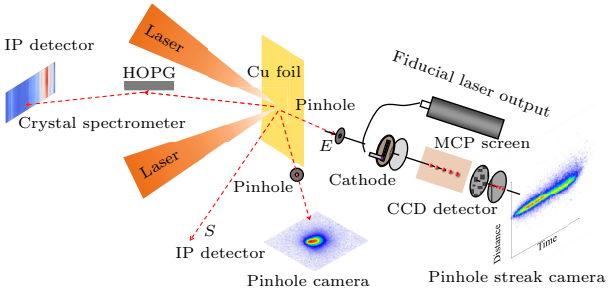


Fig. 1. Schematic diagram of the experiment setup.

Table 1. Laser parameters used in the experiments.

Shot numbers	Laser energy (J)	Focal spot size (μm)	Pulse length (ns)	Intensity (10^{14} W/cm^2)
20230228017	34	280	0.3	1.8
20230227016	165	167	1.1	6.6
20230228018	26	137	0.18	9.8

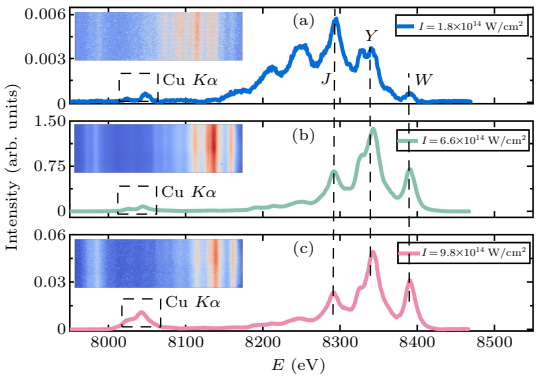


Fig. 2. Cu emission spectra measured by the HOPG crystal spectrometer at different laser intensities of 1.8×10^{14} W/cm^2 (a), 6.6×10^{14} W/cm^2 (b) and 9.8×10^{14} W/cm^2 (c).

The Cu emission spectrum obtained using the HOPG crystal spectrometer is shown in Fig. 2. Laser irradiation of metal foils typically produces two types of characteristic x-rays, generated through distinct mechanisms: inner-shell electron transitions and ion resonance line transitions. In the inner-shell transition process, electrons from neutral or weakly ionized atoms absorb energy and are ejected from inner atomic shells. The resulting vacancy is subsequently filled by an electron from a higher energy level, typically the L or M shell. This process is exemplified by the Cu $K\alpha$ spectral lines shown in Fig. 2, where Cu $K\alpha_1$ and Cu $K\alpha_2$ have central energies of 8048 eV and 8027 eV, respectively. In contrast, ion resonance line transitions occur when highly ionized atoms, with only one or two remaining electrons, undergo electronic transitions between energy levels. These transitions produce spectral lines analogous to those of low-Z elements, classified as hydrogen-like, helium-like, etc. In this study, we focus on three specific spectral lines: the resonance line of helium-like ions (W: $1s^2\ {}^1S_0$–$1s2p\ {}^1P_1$ at 8390 eV), the intercombination line (Y: $1s^2\ {}^1S_0$–$1s2p\ {}^3P_1$ at 8350 eV) and the lithium-like two-electron satellite lines (J: $1s^2\ 2p$–$1s2p^2$ at 8290 eV). Figure 2(a) presents the spectrum at a laser intensity of 1.8×10^{14} W/cm^2, where the W line exhibits weak intensity with a J/W ratio of 9.3. The spectrum is dominated by lithium-like transitions, particularly the J line and its adjacent lines of lower energies. At an increased laser intensity of 6.6×10^{14} W/cm^2 (Fig. 2(b)), helium-like transitions become predominant, as evidenced by the significant enhancement of the W spectral line and a reduced J/W ratio of 0.96, with the W line intensity slightly exceeding that of the J line. Further increasing the laser intensity to 9.8×10^{14} W/cm^2 (Fig. 2(c)) results in additional enhancement of the W spectral line, yielding a J/W ratio of 0.74, where the W line intensity substantially surpasses that of the J line. These experimental results demonstrate that the distribution of Cu ion spectral lines, particularly the J/W ratio, is closely correlated with laser–plasma interaction processes and contains valuable plasma information.[20–23] It should be noted that the HOPG spectrometer in this experiment integrates x-ray emissions from the

entire plasma volume throughout the radiation process, without spatial or temporal resolution. Therefore, the J and W line intensities reflect the integrated plasma characteristics, requiring further detailed analysis to fully interpret the underlying plasma conditions.

3. Analysis and discussion

To further elucidate the plasma characteristics via x-ray spectroscopy, a two-dimensional (2D) radiation-hydrodynamics simulation was conducted using the FLASH code.[24] The 2D axisymmetric simulation on the XY plane involved a target region, where X represents the radius direction and Y represents the height direction. The simulation box size is 300×600 μm^2, with a maximum resolution of 1.5×1.5 μm^2. The laser is incident normally along the Y-axis onto a 20 μm thick Cu target with a focus diameter of 160 μm. The simulations were tailored to model the temporal evolution and spatial distribution of temperature and density in laser-irradiated Cu foils, with parameters matching the experimental configurations. The simulation results, corresponding to a laser intensity of 6.6×10^{14} W/cm^2 and a pulse duration of 1.0 ns, are presented in Fig. 3. Figures 3(a) and 3(b) illustrate the spatial distributions of temperature and density at 0.5 ns. In Fig. 3(b), two white lines are used to represent the isodensity contours at 0.5 n_c and 1.0 n_c, where n_c denotes the critical density. Figure 3(c) shows the spatially averaged temperature and density profiles within the laser focal area, ranging from $X = -80$ μm to 80 μm. The analysis indicates that spatial averaging within the laser focal spot region has a negligible effect on the density distribution. Within the focal region, the electron temperature demonstrates a progressive increase with distance from the target surface, while the electron density exhibits a corresponding decrease. The FLASH simulation results were subsequently utilized in the FLYCHK code for spectral line calculations.

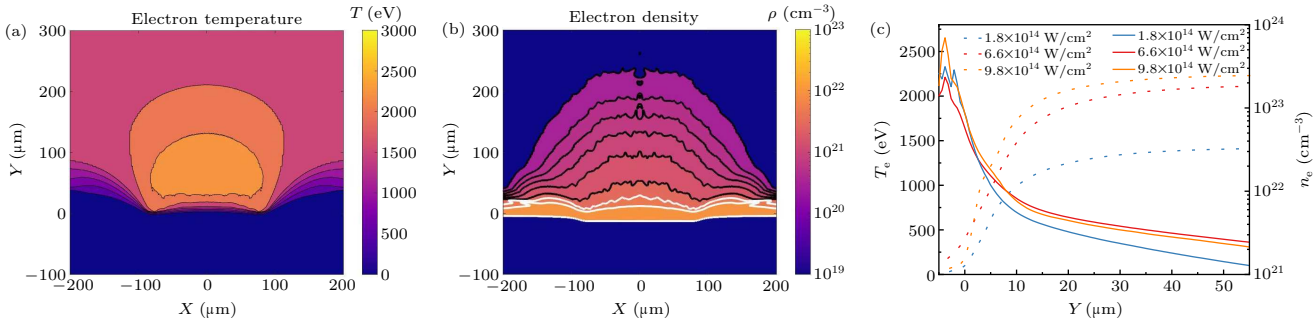


Fig. 3. [(a) and (b)] Two-dimensional spatial distributions of electron temperature and density at 0.5 ns in FLASH simulations, with a laser intensity of 6.6×10^{14} W/cm^2, respectively. (c) Averaged temperature–density distributions within the laser focal spot ($X = -80$ μm to 80 μm) for irradiation times of different laser intensities.

FLYCHK, a collisional-radiative code developed by the National Institute of Standards and Technology (NIST), models ionization state populations and line emissions by solving rate equations.[25] This code is capable of computing ionization equilibrium distributions for a wide range of elements. In this study, we employed the FLYCHK code to implement a steady-state collisional-radiative model operating under non-local thermodynamic equilibrium (NLTE) conditions, enabling the calculation of emission spectra across various temperature and density regimes. It should be noted that the research in this paper focuses on the characteristics of the plasma parameters corresponding to the Cu helium-like spectral lines. Therefore, the Cu $K\alpha$ spectral line is not included in the simulation calculation scope. The calculated spectra were subsequently convolved with a Gaussian-distributed instrument response function to account for experimental resolution effects.[26] Using the temperature and density values at different positions along the Y-axis in Fig. 3(c) as input parameters for FLYCHK, we computed the emission intensities of the J and W spectral lines under these specific conditions. The results are presented in Fig. 4(a), where the green and pink data points represent the J and W spectral lines, respectively. The analysis indicates that the emission of these spectral lines is predominantly localized within the spatial range of $Y = 7$–30 μm, corresponding to an electron density range of 0.5 n_c to 1.0 n_c. This observation suggests that the J and W spectral lines measured by the HOPG spectrometer in the experiment primarily reflect plasma conditions near the critical density surface. Given the time-integrated nature of the experimental measurements, we further conducted a statistical analysis of the temporal evolution of both the plasma temperature and the emission intensities of the J and W spectral lines in the near-critical density region. Figure 4(b) demonstrates that during laser irradiation, the plasma temperature near the critical density surface (0.5 n_c and 1.0 n_c) remains relatively stable. Similarly, the emission intensities of the J and W spectral lines exhibit negligible temporal variation, indicating a quasi-steady-state condition in this region. These findings provide valuable insight into the dynamic behavior of laser-produced plasmas near the critical density surface.

Figure 4(c) illustrates the temporal evolution of x-ray emission under a laser intensity of 6.6×10^{14} W/cm^2, captured

by a pinhole streak camera. The multiple dots at the bottom of the figure represent the time reference markers, while the central bright spots depict the one-dimensional spatial and temporal evolution of x-ray emissions. The black line corresponds to the temporal distribution of x-ray emission and the red line denotes the temporal profile of the laser pulse in Fig. 4(c). As shown in Fig. 4(c), the x-ray emission remains confined to the duration of laser irradiation, with its temporal profile closely following the laser pulse waveform. By combining the findings from Figs. 4(b) and 4(c), it can be inferred that the time-integrated J and W spectral measurements obtained from the HOPG spectrometer primarily reflect the x-ray emissions during the laser–plasma interaction period. Consequently, these measurements also provide insight into the plasma temperature near the critical density surface during the interactions. This conclusion underscores the consistency between the experimental observations and the simulated plasma dynamics, highlighting the reliability of the diagnostic approach.

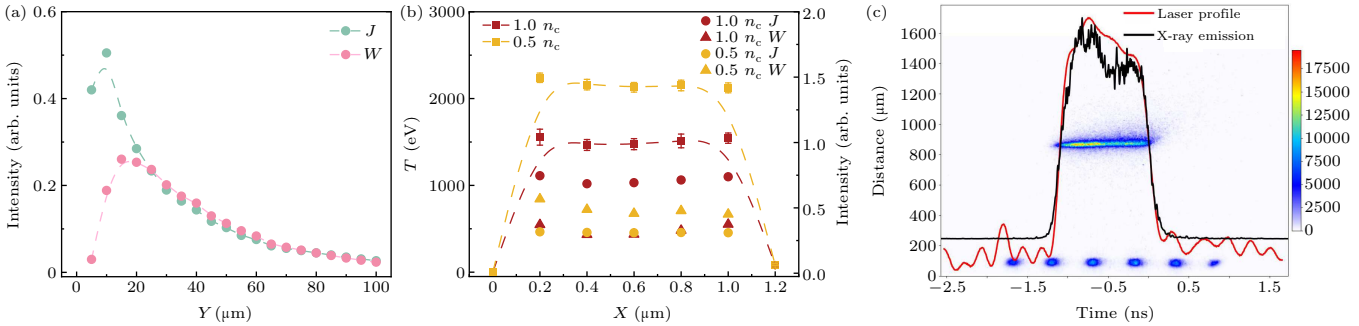


Fig. 4. (a) Variation of the emission intensity of the J and W spectral lines with respect to the Y-axis calculated by FLYCHK from the plasma temperature and density parameters given in Fig. 3. (b) Evolution of the temperature and emission intensity of the J and W spectral lines at densities of 0.5 n_c and 1.0 n_c in FLASH simulations. (c) Temporal profile of x-ray emission observed by the pinhole streak camera at the laser intensity of 6.6×10^{14} W/cm^2 .

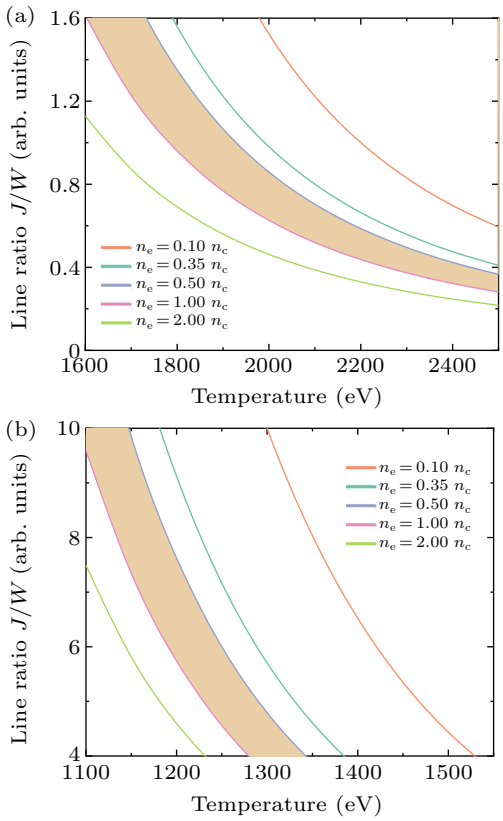


Fig. 5. The J/W ratio at different temperatures and densities calculated by FLYCHK.

Using the FLYCHK code, we conducted a series of large-scale calculations to investigate the dependence of the relative emission intensity ratio (J/W) of the spectral lines on variations in plasma temperature and density parameters. The results are presented in Fig. 5, where the calculations were performed for densities of 0.1 n_c, 0.35 n_c, 0.5 n_c, 1.0 n_c, and 2.0 n_c. As illustrated in Fig. 5, the J/W ratio exhibits a strong dependence not only on the plasma temperature but also on the plasma density. A single J/W ratio can correspond to multiple combinations of temperature and density, indicating that the J/W ratio alone cannot uniquely determine the temperature-density state of the plasma. The simulation results from the FLASH code suggest that the spectral lines measured in our experiments originate primarily from the region near the critical density surface (from 0.5 n_c to 1.0 n_c). This region is represented by the shaded area in Fig. 5.

Finally, we conducted extensive calculations using the experimentally measured J/W ratios (provided in Fig. 2) for several sets of temperature and density values selected from the shaded region in Fig. 5. These calculations aimed to determine the plasma conditions that best match the experimental spectra. The fitted spectral lines corresponding to densities of 1.0 n_c and 0.5 n_c are schematically illustrated in Fig. 6, where (a), (b) and (c) correspond to different laser intensities. The black curves represent the experimental measurements, while the blue and orange lines denote the results of FLYCHK simulations for different temperature-density conditions. The simulation results exhibit excellent agreement with the experimental data. We obtained the temperature near the critical density surface under different laser intensities, as shown in Table 2. The electron temperatures were found to be in the range of 1070 eV–1210 eV for the laser intensity of 1.8×10^{14} W/cm^2, 1810 eV–1960 eV for 6.8×10^{14} W/cm^2, and 1910 eV–2080 eV for 9.8×10^{14} W/cm^2, in the vicinity of the critical density surface (0.5 n_c to 1.0 n_c). These results demonstrate that the plasma temperature near the criti-

cal density surface increases with higher laser intensities, consistent with the electron temperature profiles obtained from the FLASH radiation-hydrodynamics simulations. Combining these findings, it is evident that the temperature of the plasma near the critical density surface during laser–plasma interactions can be reasonably inferred from experimental measurements by analyzing the intensity ratio (J/W) and the spectral line shapes in conjunction with the FLYCHK code. This approach provides a robust method for diagnosing plasma conditions in high-intensity laser experiments.

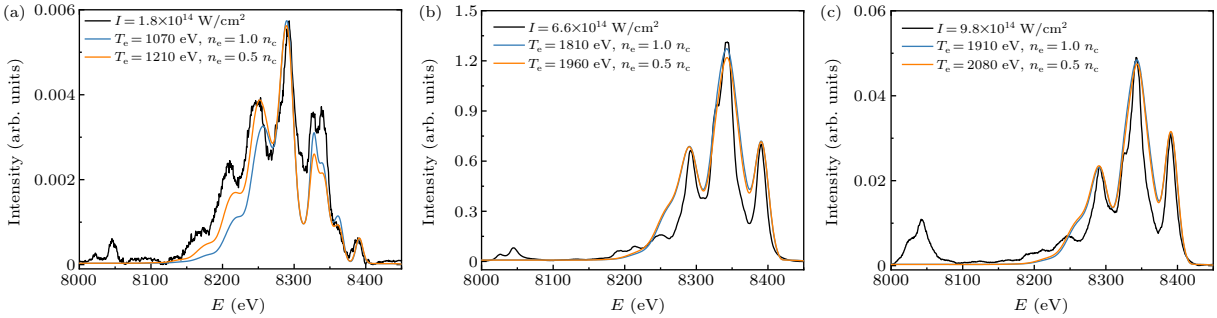


Fig. 6. (a)–(c) Comparison of the spectral lines calculated through FLYCHK simulation with those measured by the HOPG crystal spectrometer at different laser intensities.

Table 2. Temperature near the critical density surface under different laser intensities.

Laser intensity (10^{14} W/cm^2)	1.8	6.6	9.8
T (eV)	1070–1210	1810–1960	1910–2080

4. Conclusion

Experiments involving laser-irradiated Cu foils and x-ray spectroscopy diagnostics were conducted at the Shenguang-II facility. It was observed that the characteristic emission spectral lines of Cu exhibit significant variations in response to changes in laser intensity. A HOPG spectrometer was employed to measure the intensities of the J and W spectral lines. During the laser–plasma interactions, the plasma density and temperature in front of the target span a broad distribution, covering several orders of magnitude. By combining two-dimensional radiation-hydrodynamics simulation program with a spectral analysis code, the plasma information reflected by these spectral intensities was systematically extracted. The simulation results demonstrate that the measured spectral lines originate predominantly from the region near the critical density surface, with densities in the range of approximately 0.5 n_c to 1.0 n_c, and are predominantly emitted during laser pulse irradiation. Building on this finding, the plasma temperatures near the critical density surface under different laser intensities were estimated by analyzing the intensity ratios of the J/W spectral lines obtained from experimental measurements. In future experiments related to inertial confinement fusion (ICF) studies, the use of copper-doped targets combined with time-resolved x-ray spectroscopic measurements will provide a powerful diagnostic tool for investigating fast electron deposition and plasma heating processes with higher temperatures. This approach holds significant potential for advancing our understanding of high-energy-density plasma dynamics and optimizing ICF ignition strategies.

Acknowledgment

Project supported by the Strategic Priority Research Program of the Chinese Academy of Sciences (Grant Nos. XDA25051000, XDA25010100, XDA25010300, XDA25030100, and XDA25030200).

References

[1] Wu C S, Zhou F Y, Yan J, *et al.* 2024 *Chin. Phys. Lett.* **41** 085202
[2] Hammer J H, Hartman C W and Eddleman J L 1988 *Phys. Rev. Lett.* **61** 25
[3] Labaune C, Baccou C, Depierreux S, *et al.* 2013 *Nat. Commun.* **4** 2506
[4] Zhong J, Li Y, Wang X, *et al.* 2010 *Nat. Phys.* **6** 984
[5] Rogers F J and Iglesias C A 1994 *Science* **263** 50
[6] Forrest C J, Crilly A, Schwemmlein A, *et al.* 2022 *Rev. Sci. Instrum.* **93** 103505
[7] Gatu Johnson M 2023 *Rev. Sci. Instrum.* **94** 021104
[8] Fang Y L, Li D Y, Cheng H, *et al.* 2023 *Chin. Phys. B* **32** 110703
[9] He Z C, Zhang J Y, Yang J M, *et al.* 2023 *Chin. Phys. B* **32** 015202
[10] Theobald W, Solodov A A, Stoeckl C, *et al.* 2014 *Nat. Commun.* **5** 5785
[11] Zhang C L, Zhang Y H, Yuan X H, *et al.* 2024 *Chin. Phys. B* **33** 025201
[12] Walls M 2012 *Nat. Photonics* **6** 503
[13] Beier N F, Allison H, Efthimion P, *et al.* 2022 *Phys. Rev. Lett.* **129** 135001
[14] Gao L, Kraus B F, Hill K W, *et al.* 2022 *Phys. Rev. Lett.* **128** 185002
[15] Zhang J, Wang W M, Yang X H, *et al.* 2020 *Phil. Trans. R. Soc. A* **378** 20200015
[16] Dai Y, Gu H C, Fang K, *et al.* 2024 *High Power Laser Sci. Eng.* **12** e50
[17] Sakata S, Lee S, Morita H, *et al.* 2018 *Nat. Commun.* **9** 3937
[18] Liu Z D, Zhong J Y, Yuan X H, *et al.* 2023 *Chin. Phys. B* **32** 110702
[19] Dong Y F, Zhang Z, Xu M H, *et al.* 2020 *Rev. Sci. Instrum.* **91** 033105
[20] Biedermann C, Radtke R, Fournier K B, *et al.* 2002 *Phys. Rev. E.* **66** 066404
[21] Joshi T R, Bailly-Grandvaux M, Turner R E, *et al.* 2023 *Phys. Plasmas* **30** 122109
[22] Rosmej O N, Samsonova Z, Höfer S, *et al.* 2018 *Phys. Plasmas* **25** 083103
[23] Pu Y D, Zhang J Y, Yang J M, Huang T X and Ding Y K 2011 *Chin. Phys. B* **20** 015202
[24] Fryxell B, Olson R, Ricker P, *et al.* 2000 *Astrophys. J., Suppl. Ser.* **131** 273
[25] Chung H K, Chen M H, Morgan W L, *et al.* 2005 *High. Energ. Dens. Phys.* **1** 3
[26] Huntington C M, Kuranz C C, Malamud G, *et al.* 2012 *Rev. Sci. Instrum.* **83** 10